

Statistically Optimized Biopsy Strategy for the Diagnosis of Prostate Cancer

Dinggang Shen¹, Zhiqiang Lao¹, Jianchao Zeng², Edward H. Herskovits¹,
Gabor Fichtinger³, Christos Davatzikos^{1,3}

¹ Center for Biomedical Image Computing, Depart. of Radiology, Johns Hopkins University

² ISIS Center, Radiology Department, Georgetown University Medical Center

³ Center for Comp.-Integrated Surgical Systems and Tech., Johns Hopkins University

E-mails: dgshen@cbmv.jhu.edu, hristos@rad.jhu.edu

Abstract

This paper presents a method for optimizing prostate needle biopsy, by creating a statistical atlas of the spatial distribution of prostate cancer from a large patient cohort. In order to remove inter-individual morphological variability and to determine the true variability in the spatial distribution of cancer within the prostate, an adaptive-focus deformable model (AFDM) is first used to register and normalize the prostate samples. A probabilistic method is then developed to select the prostate-biopsy strategy that the greatest chance of detecting prostate cancer. For a test set of data from 20 prostate subjects, five needle locations are adequate to detect the tumor 100% of the time. Furthermore, the results on the accuracy of deformable registration and the predictive power of our statistically optimized biopsy strategy are presented in this paper.

1. Introduction

Prostate cancer is the second leading cause of death for American men [1]. When prostate cancer is diagnosed early, it is usually curable. Therefore, the decision of who and when to treat for prostate cancer is very important. Transrectal-Ultrasonography-guided symmetric needle biopsy has been widely used as a gold standard for the diagnosis of prostate cancer. However, biopsy is currently performed in a rather empirical way, since cancer is mostly undetectable in the routinely used ultrasound images. Thus, biopsy protocols that designate locations of the needles within the prostate, as well as the number of the needles to use, have been developed to help urologists perform prostate needle biopsy. The most common biopsy protocol is the systematic sextant biopsy [2]; however, recent studies have shown that this protocol produces a positive predictive value of only 20-30% [3], which results in a significant number of prostate-cancer cases being undetected at initial biopsy.

Researchers have investigated the possibility of using a large number of patient histopathological images to determine prostate regions that are most likely to develop cancer, and therefore should be sampled during biopsy [4]. Those techniques, however, are limited by two factors: inter-individual morphological variability, and statistical models that do not investigate correlation among different prostate areas. In this paper, we present methods that overcome both of these limitations. In order to reduce inter-individual variability, we use deformable models [5,6], which spatially normalize the prostate images to a canonical coordinate system with high accuracy. After accurate registration of the prostate images of a large number of patients, a full statistical atlas

of cancer distribution is created, and applied to optimization of biopsy strategy. With regard to the statistical analysis, we consider not only the probability of developing cancer at individual locations; rather, we employ a full statistical predictive model that takes into account the spatial correlations of cancer incidence among different prostate regions. Our rationale is that regions for which cancer incidences are very highly correlated need not be sampled simultaneously, as opposed to regions for which cancer occurrences are relatively independent. These models will be used as an optimization framework for generating a patient-specific needle biopsy strategy. Fig. 1 demonstrates our ideas schematically. In Section 2 we introduce our method for normalization of prostate images using deformable registration and warping algorithms. Section 3 presents our probabilistic method for optimizing biopsy strategy based on a probabilistic spatial prostate-cancer atlas. We present the results of evaluation of these techniques in Section 4. This paper concludes in Section 5.

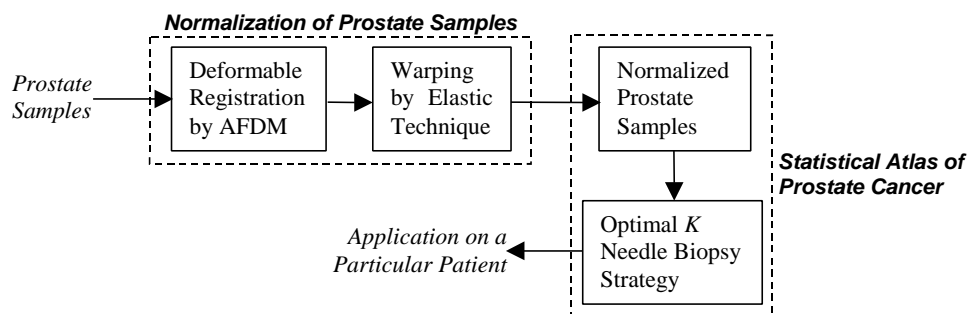


Figure 1. A schematic representation of our method for the diagnosis of prostate cancer.

2. Normalization of prostate samples

The major problem in developing a spatial normalization method for prostate samples is determining point correspondences among the samples. We have developed a deformable shape-modeling framework, for segmentation of anatomical shapes, and for determining point correspondences across individuals, from tomographic images [5,6]. This framework is based on our *adaptive focus deformable model* (AFDM). In AFDM, for a given set of structures, shape models are first constructed to represent the average shapes of these structures. These shape models include two kinds of information: information about the geometry of the structures, and information about the statistical variation of these structures within a given population. In the application stage, the deformable shape model is superimposed on an image, and subsequently set free to deform according to features extracted from the images, seeking objects that have similar geometry and that fall within the expected range of shape variation.

AFDM is used here to register the external and internal structures of the prostate images, (i. e., the capsule and the urethra.) We select one typical prostate data set as a template (Fig. 2a), and other subjects are warped into the space of this template. The warping process is performed in two stages. First, AFDM is used to reconstruct the shape of each structure and to determine point correspondences between the subject and the template. Second, these point correspondences are interpolated elsewhere in the space of the template by using an elastic-warping technique [7].

Our prostate template has two surfaces that respectively represent the capsule and the urethral boundaries (Fig. 2a). In order to allow deformation imposed on a segment of the capsule surface to rapidly propagate to the segments of the urethral surface, the new

connections between these two surfaces are inserted as gray arrows shown in Fig. 2b. Furthermore, in order to capture the geometry of anatomical structures in a hierarchical fashion, we employ an attribute vector [6] that is associated with each point of the prostate model, which reflects the geometric structure of the model from a global scale to a local scale. Local-scale attributes reflect differential geometric characteristics of the underlying structure, such as curvature, while global-scale attributes capture spatial relationships among distant points. The attribute vectors are an important aspect of AFDM, since they provide a means for finding correspondences across individuals by examining the similarity of the underlying attribute vectors. In the 3D case, each attribute is defined as the volume of a tetrahedron.

Fig. 3 demonstrates an example of registering and warping prostate image data for a typical subject (Fig. 3(b1)) to the space of the template (Fig. 3(a1)). Figs. 3(a1) and 3(b1) display the same views of the template and the subject. The spatially normalized version of the subject is shown in Fig. 3(c1). Fig. 3(a2) shows a selected cross-sectional image of the template. The corresponding cross-sectional image of the subject is shown in Fig. 3(b2). Note the shape differences between these two cross sections. After using our warping algorithm, we obtain the warped cross-sectional image in Fig. 3(c2), whose shape is very similar to that of the template in Fig. 3(a2).

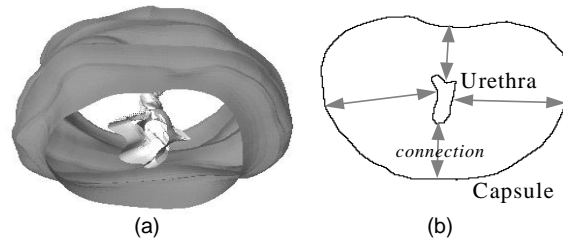


Figure 2. A 3D prostate model with two surfaces that represent the capsule and the urethral boundaries, respectively. (a) 3D display, and (b) cross-section.

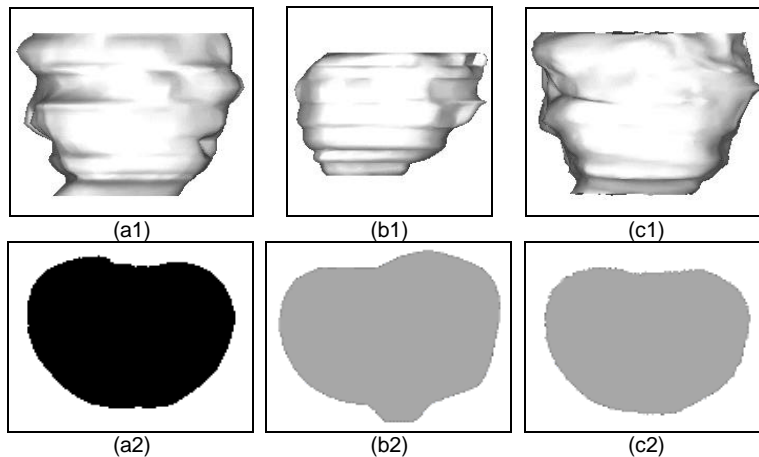


Figure 3. An example of normalizing a prostate subject to the space of the template. (a1) A side view of the prostate template to which all subjects are warped, (b1) a side view of a selected subject, (c1) a side view of the normalized subject. Figs. (a2-c2) are the representative cross-sectional images, corresponding to (a1-c1).

3. Optimized needle-biopsy strategy

With the prostate subjects warped to the space of the prostate template, we are ready to calculate the 3D statistical atlas of prostate cancer location, and to use this

probabilistic atlas to generate an optimized needle-biopsy strategy for a given patient. In this paper, we assume that at the needle tip we collect only one voxel of tissue. In reality, the harvested tissue sample is a small cylinder cutting across many voxels. We will expand the method from ‘needle tip biopsy’ to ‘cylindrical core biopsy’ in the future. In the following, we describe an algorithm to design an optimal K -biopsy (biopsy with a number of needles K) strategy by minimizing the probability of missing the cancer on all biopsies.

Optimization: A K -biopsy strategy can be optimized by minimizing the probability that none of the K needles detect cancer. This probability is defined as

$$P(B(x_i) = \text{NC}, i = 1, \dots, K), \quad (1)$$

where $B(x_i)$ is the biopsy outcome at location x_i , and NC denotes a negative cancer-detection result. Location x_i can be anywhere inside the 3D prostate template. We can find the configuration that minimizes this probability by using standard optimization methods. Since the probability in (1) is likely to have many local minima, the simulated-annealing technique is used to find the optimal locations of all needles. We start with an initial guess for the coordinates of the K needles, based on the spatial prevalence (i. e. marginal probability) of prostate cancer, and then we iteratively change these values in a direction that decreases the probability function (1). Initially, changes in the direction that increases the probability function are allowed, but these steps are progressively discouraged as the algorithm proceeds, as is customary in nonlinear-optimization methods.

Initialization: The search space in our optimization problem is very large, since each of the K needle coordinates can be at any voxel within the prostate template. Therefore, in order to make the simulated-annealing technique practical, we need to find a good initial guess for the starting point for this algorithm. Here, we describe a very fast heuristic method, which we have implemented based on 20 of the 281 prostate datasets. It does not always guarantee to find the global minimum, although in our preliminary experiments with 20 subjects it did find the globally optimal solution. In the following, we describe this fast initialization method.

The probability of missing cancer can be expressed as a product of conditional probabilities,

$$P(B(x_i) = \text{NC}, i = 1, \dots, K) = P(B(x_1) = \text{NC}) \times P(B(x_2) = \text{NC} \mid B(x_1) = \text{NC}) \times \dots \times P(B(x_K) = \text{NC} \mid B(x_i) = \text{NC}, i = 1, \dots, K-1). \quad (2)$$

Our heuristic method sequentially minimizes a series of the conditional probabilities of missing cancer, each of them being one of the terms in (2) above. Suppose there are N different locations in the prostate template, and M prostate samples in the training set. To minimize (2), one of the K biopsies, let’s say the first biopsy $B(x_1)$, will be taken from the location x_1 where the spatial prevalence of cancer is greatest, or, equivalently, the first term in (2), $P(B(x_1) = \text{NC})$, is minimal. Knowing the location of the first biopsy x_1 , in order to calculate the conditional probability $P(B(x_2) = \text{NC} \mid B(x_1) = \text{NC})$, we remove those prostate samples that have cancer at the location x_1 , since those do not satisfy the condition $B(x_1) = \text{NC}$, and calculate the conditional probability for each location. It is important to note that if the prevalence of cancer at a location other than x_1 is strongly associated with the prevalence of cancer at location x_1 , then the cancer occurrence probability of this location will become very low in the conditional probability $P(B(x_2) = \text{NC} \mid B(x_1) = \text{NC})$. This is because all subjects with cancer at x_1 have been excluded in calculating the conditional probability $P(B(x_2) = \text{NC} \mid B(x_1) = \text{NC})$. This implies that the second biopsy will most likely not be placed at locations strongly

associated with location x_1 . Analogous to the procedure for determining the optimal location x_1 , the optimal location x_2 can be determined by minimizing the conditional probability $P(B(x_2)=NC \mid B(x_1)=NC)$. Using the same procedure, the locations of other biopsy sites can be similarly determined. This procedure is efficient, since it doesn't operate on the full-joint distribution. Effectively, regions for which cancer prevalence strongly correlated will not be sampled simultaneously, whereas regions for which cancer occurrences are independent are more likely to form an optimal biopsy strategy.

4. Experiments

We performed two sets of experiments in order to test the performance of our deformable registration, and as well as to validate the predictive power of our atlas-based optimal biopsy strategy in detecting prostate cancer. These two sets of experiments were performed on 20 of the 281 prostate subjects in our database.

Registration accuracy of our AFDM: We measured the percent overlap and average distance between prostate structures in 20 images and their counterparts in the template, after all prostate subjects were warped to the space of the template. Note that these images are all labeled, and therefore the overlap percents of the various prostate structures across subjects can be readily computed. For 20 prostate images, the overlap fractions range from 97.6% to 98.4%, with a mean of 98.2%. The average boundary distances range from 1.7 to 2.1 pixels. Since our prostate template is represented by an image with the size of 256x256x124 pixels, these average boundary distances are therefore much smaller.

Positive predictive value of the optimized biopsy strategy: Using our registration and warping algorithm, we can eliminate most of the overall shape differences across individuals, and can therefore compute the spatial distribution of cancer; we use this distribution for generating an optimal needle-biopsy strategy. We tested the heuristic sequential optimization procedure on 20 subjects. All 256x256x124 voxels were considered to be candidate biopsy locations. In Fig.4a, the optimized biopsy sites are shown as small spheres and the underlying spatial statistical distribution of cancer is shown as gray-scale, where a brighter voxel represents a higher probability of finding cancer in that location. A typical cross-section of the spatial prostate-cancer probability distribution is shown in Fig. 4b. Five needles were adequate to detect the tumor in 100% of the 20 subjects. The locations of these five needles, with depth information, are shown in Fig. 4c. Of course, this strategy will almost certainly change as we increase the number of subjects. However, an important implication of these results is that optimized needle placement is not necessarily on regions that have high likelihood of cancer. As we can see from Fig. 4a, only the first two needles were placed in brighter gray-scale (high-prevalence) regions; the rest were placed in regions that were almost independent of the first two. In addition, we validated the predictability of our biopsy strategy by using a leave-one-out method, which also showed the rate of success to be 100%.

5. Conclusion and future work

We have presented a method for creating a statistical atlas, and for using this atlas to guide the optimization of a needle-biopsy strategy. We tested this method using image data from 20 subjects; we will extend this work to the entire database of 281 subjects.

We will also develop a method for rapid warping our statistical atlas to real-time transrectal ultrasound, which is currently the predominant imaging technique in prostate biopsy. Successful implementation of this data fusion process is expected to improve the overall predictive accuracy of prostate biopsy, and may also assist in deciding the appropriate course of treatment.

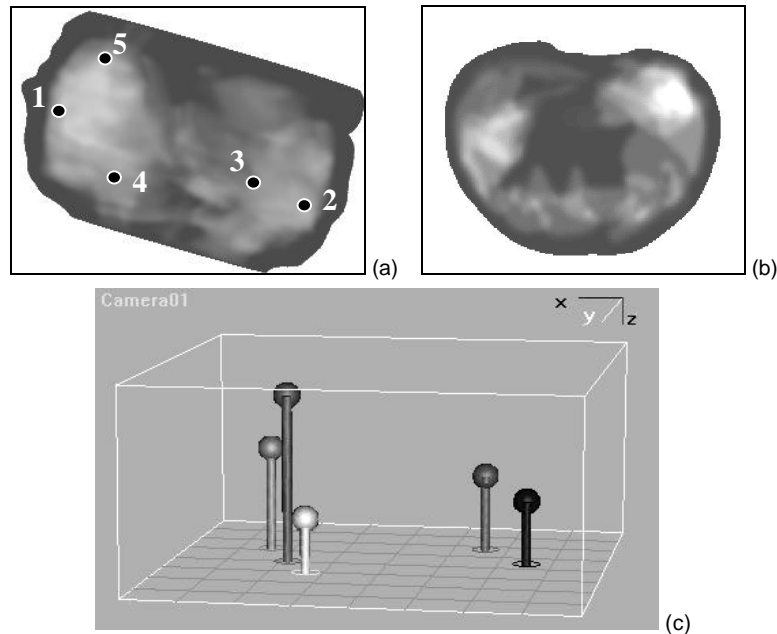


Figure 4. Optimal biopsy strategy using a statistical atlas of cancer distribution. The 5 biopsy positions are shown as spheres in (a), with the statistical atlas of cancer shown as gray level. A typical cross-sectional image of the statistical atlas of cancer is shown in (b), and the locations of five needles with depth information are shown in (c).

Acknowledgments: We thankfully acknowledge the collaborations of John Bauer (Walter Reed Army Medical Center), Wei Zhang and Isabell Sesterhenn (Armed Forces Institute of Pathology), Judd Moul (Center for Prostate Disease Research), and Seong K. Mun (Georgetown University Medical Center). This work was supported in part by a grant from the National Science Foundation to the Center for Computer Integrated Surgical Systems and Technology. J. Zeng was supported by the Whitaker Foundation.

References:

1. C. Bohring, and T. Squires. Cancer statistics. *CA Cancer J. Clin.*, vol. 43, pp. 7-26, 1993.
2. K.K. Hodge, J.E Mcneal, M.K. Terris, T.A. Stamey. Random systematic versus directed ultrasound guided trans-rectal core biopsies of the prostate. *J. Urol.*, 142: 71-74, 1989.
3. R.C. Flanigan, W.J. Catalona, J.P. Richie, *et al.* Accuracy of digital rectal examination and transrectal ultrasonography in localizing prostate cancer. *J. Urol.*, 152: 1506-1509, 1994.
4. J. Zeng, J.J. Bauer, A. Sofer, X. Yao, B. Opell, W. Zhang, I.A. Sesterhenn, J.W. Moul, J. Lynch, S.K. Mun. Distribution of prostate cancer for optimized biopsy protocols. *MICCAI*, Pittsburgh, Oct. 2000.
5. D. Shen, C. Davatzikos. An adaptive-focus deformable model using statistical and geometric information. *IEEE Trans. on PAMI*, 22(8):906-913, August 2000.
6. D. Shen, E.H. Herskovits, and C. Davatzikos. An adaptive-focus statistical shape model for segmentation and shape modeling of 3D brain structures. *IEEE Trans. on Medical Imaging*, 20(4), April 2001.
7. C. Davatzikos. Spatial transformation and registration of brain images using elastically deformable models. *Comp. Vis. and Image Understanding*, 66(2):207-222, May 1997.